

Quantifying Graphite Solid-Electrolyte Interphase Chemistry and its Impact on Fast Charging

Eric J. McShane^{1,2}, *Helen Bergstrom*^{1,2}, *Peter J. Weddle*³, *David E. Brown*^{1,2}, *Andrew M. Colclasure*³,
Bryan D. McCloskey^{*,1,2}

¹Department of Chemical and Biomolecular Engineering, University of California, Berkeley, California 94720, United States

²Energy Storage and Distributed Resources Division, Lawrence Berkeley National Laboratory, Berkeley, California 94720, United States

³Energy Conversion and Storage Systems Center, National Renewable Energy Laboratory, Golden, Colorado 80401, United States

*Corresponding Author; E-mail: bmcclosk@berkeley.edu

Abstract

The solid-electrolyte interphase (SEI) enables the remarkable capacity retention of lithium-ion batteries, yet a comprehensive quantitative description of the SEI composition remains elusive. Using a combination of differential electrochemical mass spectrometry and mass spectrometry titration, we quantify graphite SEI components formed under electrolytes of varying salt concentrations. We find that, regardless of salt concentration, a conversion of initially deposited lithium ethylene dicarbonate to monocarbonates (likely lithium ethylene monocarbonate) and non-carbonate species occurs, and the extent of this conversion increases with electrolyte aging. We additionally demonstrate that as concentration increases (up to 2.0 M LiPF₆), the SEI becomes progressively thinner with more LiF and less solid carbonates deposited. Finally, we reveal that less dead lithium formation and less solid carbonate deposition occurs during prolonged fast charging for higher concentration electrolytes. Owing to the advantages imparted by a thinner SEI, the onset state of charge for lithium plating for the 2.0 M electrolyte is later than that predicted by a standard electrochemical model, underscoring the importance of explicit SEI effects in future electrochemical models.

The solid-electrolyte interphase (SEI), a nanometer-scale layer comprised of electrolyte salt and solvent degradation products, plays a pivotal role in lithium-ion battery (LIB) operation. A well-formed SEI must be both ionically conductive and electronically insulating to allow Li⁺ transport to the electrode surface while preventing continual solvent reduction. As such, significant research effort has focused on tuning electrolyte composition to impart optimal SEI properties. However, despite its recognized importance, characterization of the SEI is often limited to qualitative techniques, such as X-ray photoelectron spectroscopy (XPS, which can provide the atomic ratios of various elements in the SEI layer) and Fourier transform infrared spectroscopy (FTIR, which can provide information about functional groups present in the SEI). There remains a pressing need for quantitative studies of SEI composition, especially because such studies can elucidate the extent of specific capacity loss mechanisms during cycling.

In this work, we develop a quantitative understanding of the SEI composition —both during initial formation cycling and after fast charge cycling —through the use of operando differential electrochemical mass spectrometry (DEMS) and ex-situ mass spectrometry titration (MST) measurements (detailed in Supporting Information Section S1). Noting that both the electrolyte solvent and the Li⁺ counteranion are known to degrade to form the SEI, [1] varying the salt concentration in an electrolyte will ultimately impact the SEI composition. We therefore studied electrolytes with a range of salt concentrations, from 0.35 M LiPF₆ to 2.0 M LiPF₆, always in a solvent blend of 3:7w ethylene carbonate (EC) to ethyl methyl carbonate (EMC). We quantified gas evolution, specifically H₂, C₂H₄, and CO₂, during the first formation cycle of a graphite electrode using DEMS. Given trends observed when aging an electrolyte prior to cell preparation (see Supporting Information Section S2), we argue that H₂ evolution is a proxy for LiF formation, allowing us to approximate the LiF content in the SEI. C₂H₄ evolution results from EC reduction to form lithium ethylene dicarbonate (LiEDC), and CO₂ likely evolves from a slow chemical process that converts LiEDC, a dicarbonate, to lithium ethylene monocarbonate (LiEMC), a monocarbonate. Additionally, we perform MST to quantify the total amount of solid carbonate species present in the SEI, as well as total Li metal plated during fast charge to various states of charge and cycle numbers. By comparing C₂H₄ evolution in operando DEMS analysis to the total solid carbonates in the SEI measured by MST, we argue that a mixture of LiEDC and LiEMC is present in the SEI, and the ratio of LiEDC to LiEMC changes as a function of electrolyte aging time. As anticipated, we found that varying the

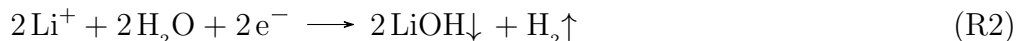
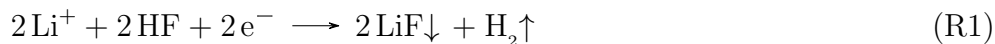
electrolyte salt concentration significantly altered the formed graphite SEI composition, with higher salt concentration electrolytes resulting in a more LiF-rich and solid carbonate-poor SEI compared to lower concentration electrolytes. This change in SEI composition also affected the fast charge behavior, with the 2.0 M electrolyte showing a delayed onset for Li plating compared to that predicted by a standard electrochemical model. With this in mind, we highlight the need for more advanced electrochemical models with explicit SEI effects. Finally, higher concentration electrolytes resulted in less dead Li (defined here as plated Li and lithiated graphite which are not electrochemically active) and less solid carbonate deposition during prolonged fast charge cycling, albeit with increased capacity fade (likely due to LiF deposition during fast charge) compared to the lower concentration electrolytes. Our findings can guide the design of emerging electrolyte compositions tailored for fast charge-capable LIBs.

Differential Electrochemical Mass Spectrometry and Mass Spectrometry Titration. Differential electrochemical mass spectrometry (DEMS) allows one to quantify gas evolution in operando during electrochemical cycling. The measurements in this work were performed using a custom built DEMS instrument and custom cells that have been described in depth elsewhere. [2] Electrolytes of 0.35 M, 0.70 M, 1.2 M, and 2.0 M LiPF_6 concentration were cycled in Li-graphite DEMS cells with a single C/10 (based on 350 mAh/g reversible graphite capacity) formation cycle with lower and upper cutoff potentials of 0.010 V and 1.5 V. The evolution rates of three gases (H_2 , C_2H_4 , and CO_2) were measured and quantified by comparison to calibration curves generated using various analyte gas/argon mixtures. Besides H_2 , C_2H_4 , and CO_2 , no other gases were observed in measurable quantities (noting a gas detection sensitivity of our DEMS to be roughly 0.05 nmol/min). Prior studies have reported other gases (e.g., CH_4 and C_2H_6) evolved in full cells with NMC cathodes, [3] but prior studies of graphite half cells typically report only H_2 , C_2H_4 , and CO_2 . [4–7] We suspect that crosstalk between the electrodes may influence the gassing behavior of full cells compared to half cells. Further details regarding DEMS measurements can be found in Supporting Information Section S1.

Mass spectrometry titration (MST) was used to quantify SEI species on cycled graphite electrodes ex-situ. A detailed description of the technique can be found in a previous publication. [8] Electrodes from both coin cells and DEMS cells were extracted from cells and titrated after proper rinsing in dimethyl carbonate (see Supporting Information Section S1). After rinsing, the electrode sample was placed in a titration vessel, the vessel was connected to an in-line mass spectrometer (all the while remaining air-free), and 3.5 M H_2SO_4 (which was previously found to provide sufficient acid strength to fully react with all solid carbonate species) [2] was injected into the vessel. The acid reacted with SEI species, including dead Li, solid carbonates, and Li_2C_2 , present on the electrode to evolve H_2 , CO_2 , and C_2H_2 gas, respectively. With appropriate calibration of each gas as described previously, [8] the amount of gas and therefore the amount of each SEI species was quantified. Chemical reactions involving each class of species with the acid titrant can be found in Supporting Information Section S1. The amount of Li_2C_2 formed was generally small in all samples tested, and further information about a possible formation mechanism for this species along with the full set of Li_2C_2 quantification data can be found in Supporting Information Section S3.

Origins of Hydrogen Evolution. Figure 1a shows the formation cycle voltage profile for a DEMS cell (a Li metal electrode and porous graphite electrode with 1.2 M LiPF_6 electrolyte) cycled at C/10. The inset of Figure 1a reveals that H_2 begins to evolve slightly before C_2H_4 , and the magnitude of H_2 evolution is significantly less than that of C_2H_4 . This implies that the product of the H_2 -forming reaction (which we will soon argue is predominantly LiF) deposits first on the graphite surface. Additionally, the C_2H_4 evolution rate surpasses the H_2 evolution rate only after H_2 evolution begins to attenuate. We propose that the deposited LiF layer covers much of the graphite surface at early stages of formation cycling, and EC reduction (resulting in C_2H_4 evolution and solid carbonate deposition) occurs on any remaining exposed graphite surface area slightly later in the formation cycle. This results in a thin layer of LiF (confined to the inner-SEI) and a thicker layer of solid carbonate species (which are interspersed with LiF in the inner-SEI and are the major constituents of the outer-SEI).

Hydrogen evolution can occur from the reduction of HF (to form LiF, see Reaction R1) and H_2O (to form LiOH and Li_2O , see Reactions R2 and R3) at the lithium metal counter electrode or at the partially lithiated graphite electrode.



However, the hydrogen evolution peak observed in Figure 1a and b is entirely related to processes occurring at the graphite electrode, as prior work confirms that no gas evolution occurs when stripping Li metal from the counter electrode. [9] The SEI on Li is formed upon initial cell construction (and thus any resultant gas formation would not be captured by DEMS), whereas the SEI on graphite is formed during formation cycling. To understand the chemical origin of H_2 , it is important to consider the effect of electrolyte aging prior to placing it in a cell, which affects the speciation of components within the electrolyte. Trace water impurities (which are inevitably present in battery electrolytes) can react with both electrolyte salt and solvent species over the course of weeks to months after the salt and solvent are mixed in a glovebox, and the new species formed in solution can change the gassing behavior. [10–12] For example, water reacts in the presence of LiPF_6 to form HF according to Reactions R4 and R5.



The molecular dissociation of LiPF_6 (Reaction R4) is reasonably sluggish in typical battery electrolytes, but the presence of water quickly consumes any PF_5 that forms, driving Reaction R4 further forward. [13] One study found that even after the intentional addition of 1000 ppm H_2O (battery electrolytes typically contain less than 50 ppm H_2O) to a 1.0 M LiPF_6 in 1:1v EC to diethyl carbonate (DEC) electrolyte, ~65% conversion of LiPF_6 to HF occurred only after about one week. [10] This suggests that the calendar age of the electrolyte plays an important role in the speciation of electrolyte components. We also found, using DEMS, that gas evolution was significantly impacted by the age of the electrolyte, as is shown in Supporting Information Section S2 and discussed below. We note that no distinguishable POF_3 signature was observed (via Reaction R5) during DEMS experiments, indicating that the impact of electrolyte aging over the course of a single DEMS experiment (~1 day) was negligible.

The inset of Figure 1a shows that H_2 is the first gas to evolve after cycling commences, and Figure 1b shows that H_2 evolution primarily occurs in the first ~3 hours of C/10 formation. The electrolyte used in Figure 1 was aged for one week in a vial with electrical tape around the cap and stored in an Ar glovebox (such that no further water contamination was possible) prior to cell preparation. Interestingly, we found that after the same electrolyte had been aged for about three months, it exhibited about four times more H_2 evolution compared to Figure 1 (see Supporting Information Section S2). Karl Fischer titration measurements on freshly-made and aged electrolytes indicated that the initial water content in tested electrolytes was ~10 ppm (~33 nmol H_2O in 60 μL of electrolyte), and the water content decreased to ≤ 5 ppm (~17 nmol H_2O in 60 μL of electrolyte) after about a week (presumably due to consumption of H_2O via Reactions R4 and R5), after which it remained stable at < 5 ppm for the next several weeks (see Supporting Information Section S2). We note that 5 ppm was the lower end of the reliable detection range for the Karl Fischer apparatus used (Metrohm Titrando with oven), so the true water content may actually have been below this value.

By integrating the total H_2 evolved in Figure 1b, we find that ~65 nmol of H_2 was evolved from the 12 mm diameter graphite electrode (3.2 mAh total nominal capacity). Considering Karl Fischer measurements

indicated that at most 17 nmol of H₂O was present in the electrolyte after one week of aging, we propose that H₂ evolution coincides predominantly with HF reduction (as illustrated in the inset of Figure 1b and shown in Reaction R1) rather than H₂O reduction (see Reaction R2). This conclusion is consistent with previous studies of graphite SEI composition, which typically report a LiF-rich inner-SEI with sporadic LiOH and Li₂O content. [14,15] Since two moles of LiF are deposited per one mole of H₂ evolved, we expect ~130 nmol of LiF were deposited from HF reduction, corresponding to a fully compact LiF layer of about 0.5 nm, or 1-2 monolayers of LiF, on the graphite particles (see Supporting Information Section S4). Prior reports suggest that LiF can also be deposited via the direct reduction of LiPF₆, but this mechanism would result in PF₅ gas evolution, which we do not observe in DEMS measurements. [16] Notably, the measured amount of H₂ evolved (65 nmol) exceeds the amount that would be expected from H₂O present even in a freshly made electrolyte (at most 33 nmol H₂O when fresh, corresponding to 17 nmol H₂ evolved). This implies that some portion of the LiPF₆ salt may have been converted to HF via a reaction with electrolyte solvent, rather than via a reaction with H₂O. Finally, given the drastic increase in DEMS H₂ evolution upon aging and the relatively small water content in the electrolytes, it is likely that another unknown mechanism besides LiPF₆ hydrolysis results in additional HF or other protic species formation during electrolyte aging (see Supporting Information Section S2).

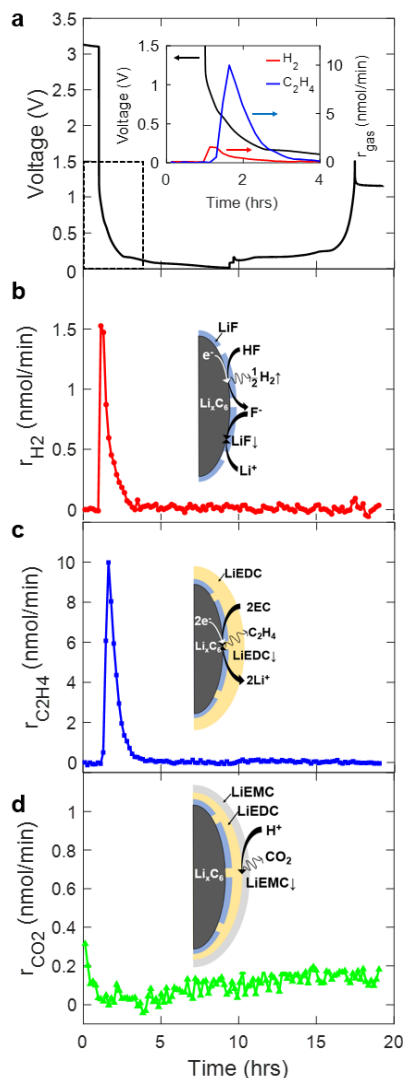
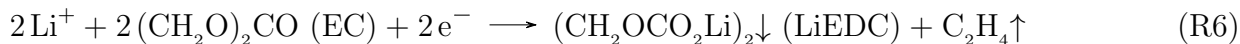
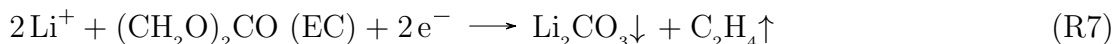


Figure 1: DEMS measurements for the formation (first) cycle of a Li-graphite cell with 1.2 M LiPF₆ in 3:7 wt:wt EC:EMC electrolyte. **a.** Voltage profile for the first C/10 cycle, with inset showing H₂ (red, onset at ~0.90 V) and C₂H₄ (blue, onset at ~0.70 V) gas evolution during the first 4 hours. **b.** H₂ gas evolution rate (r_{H_2}) with inset showing LiF deposition mechanism (see Reaction R1). A total of 65 nmol H₂ was evolved. **c.** C₂H₄ gas evolution rate ($r_{C_2H_4}$) with inset showing LiEDC deposition mechanism (see Reaction R6). A total of 496 nmol C₂H₄ was evolved. **d.** CO₂ gas evolution rate (r_{CO_2}) with inset showing LiEMC chemical formation mechanism (see Reactions R10 and R11). A total of 80 nmol CO₂ was evolved after the 5 hour mark.

Origins of Ethylene Evolution. Ethylene evolution has been proposed to primarily arise from the reduction of EC to form LiEDC, according to Reaction R6, although recent studies suggest LiEDC may undergo further reaction with protic species once initially deposited. [17] The onset of C₂H₄ evolution occurs slightly after the onset of H₂ evolution, as shown in the inset of Figure 1a, and it persists for about 4 hours, as shown in Figure 1c. This C₂H₄ evolution coincides with the formation of the outer-SEI, which is rich in alkyl carbonates, such as LiEDC. By integrating the C₂H₄ evolution signature, we found a total of 496 nmol C₂H₄ was evolved, which would correspond to a fully compact LiEDC layer of 14 nm (see Supporting Information Section S4). We note this is significantly thicker than the ~0.5 nm LiF layer calculated from the total H₂ evolved. Combining the expected capacity losses resulting from both H₂ and C₂H₄ evolution, we calculate ~1% capacity loss during the first formation cycle due to gassing reactions, compared to the observed ~6% capacity loss during the first cycle. We suspect the remaining ~5% capacity loss is due to further reduction of the LiEDC once deposited (e.g., to lithium oxalate or Li₂C₂) [18, 19] and the presence of dead lithiated graphite particles due to the volumetric expansion and subsequent dislodgement of graphite particles during initial cycling.

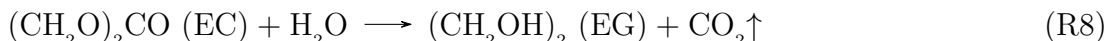


We note that another mechanism (Reaction R7) by which C_2H_4 is evolved has been previously proposed, where Li_2CO_3 forms from EC reduction instead of LiEDC. [20] However, the abundance of alkyl carbonates in multiple characterized SEI films suggests that Reaction R6 occurs to a far greater extent than Reaction R7. [1, 15, 21, 22] Battery aging and cycling conditions may affect the speciation of SEI components as well, as more 'inorganic' SEI components (including Li_2CO_3) are often reported after higher temperature cycling and prolonged battery aging. [23, 24]



Origins of Carbon Dioxide Evolution. Figure 1d shows that some CO_2 is evolved during the initial rest period, and after about five hours, a steady (albeit small) rate of CO_2 evolution is again observed. This CO_2 evolution is likely chemical, rather than electrochemical, in nature, as it remains relatively constant when the current is switched between reduction and oxidation at ~ 9 hrs, as well as during the final open circuit voltage stage starting at ~ 17 hrs. As will be described below, the initial CO_2 evolution likely arises from the reaction of EC with water or OH^- (which can be produced via the reduction of electrolyte components at the Li counter electrode during rest), while the steady evolution of CO_2 later in cycling likely arises due to the reaction of LiEDC with H_2O and HF to form LiEMC, which is illustrated in the inset of Figure 1d. This observation also suggests that not all H_2O and HF initially present in the electrolyte are consumed during inner-SEI formation, implying that the formation of the inner-SEI self-passivates. The Figure 1d inset depicts the LiEDC-to-LiEMC reaction front beginning from the outermost portion of the LiEDC layer and gradually moving inwards. We will further justify this mechanism using a combination of DEMS and MST results later in this manuscript.

During the initial open circuit voltage, CO_2 evolution can occur when EC is directly hydrolyzed by water or reacts with hydroxide (OH^-), which may be present due to trace water or electrolyte reduction at the Li metal counter electrode. [4, 11, 25, 26] Both EC reaction pathways evolve CO_2 , as shown in Reactions R8 and R9.



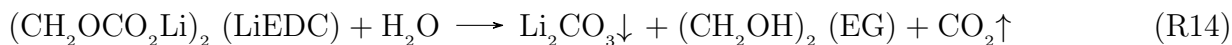
Another source of CO_2 evolution is the chemical reaction of existing graphite SEI components with H_2O and HF once the SEI has been formed (i.e., after the initial few hours in Figure 1). [26] As discussed earlier, a common graphite SEI component formed under EC-containing electrolytes is LiEDC. This species, despite its frequent mention in the SEI literature over decades, [21, 27] was only successfully chemically synthesized in 2019, [17] although LiEDC was correctly identified on a nickel substrate after electrochemical reduction of EC many years prior. [27] Previous attempts at chemically synthesizing LiEDC had actually synthesized LiEMC, [28–30] and this called into question the true chemical composition of the graphite SEI. Wang et al. posited that LiEDC forms initially but is converted to LiEMC via an unknown mechanism. [17] A key finding of our work is that LiEDC is prone to react with both H_2O and HF via the proposed Reactions R10 and R11 to form LiEMC and in the process evolve CO_2 . We attribute the steady evolution of CO_2 starting at ~ 5 hrs in Figure 1d to this process. A total of 80 nmol of CO_2 is evolved after the 5 hr mark, which corresponds to a $\sim 8\%$ reduction in the amount of solid carbonates due to the conversion of LiEDC to LiEMC if the CO_2 were entirely attributed to Reactions R10 and R11. Our proposed mechanism of LiEDC-to-LiEMC conversion is further supported by the three-month aged electrolyte discussed in Supporting Information Section S2, which exhibited a fourfold increase in CO_2 evolution (excluding the initial rest period) compared to the one-week aged electrolyte portrayed in Figure 1.



LiEMC may also undergo an additional protonation with H_2O or HF to form EG and evolve yet another CO_2 as shown in Reactions R12 and R13.



However, there remains debate about the exact reaction mechanism involving SEI components and H_2O or HF . Reaction R14, for example, shows a previously proposed double protonation of LiEDC reaction mechanism which results in Li_2CO_3 . [26] Since Li_2CO_3 is typically reported to be either not present at all [22,31,32] or confined to the inner-SEI, [14,33] and the reaction of LiEDC with H_2O or HF would occur starting from the outermost-SEI and proceed inwards (as discussed earlier), we propose that sequential protonation from LiEDC to LiEMC to EG (as described in Reactions R10-R13) is more likely.



It should also be noted that full cells with transition metal oxide cathodes may further exacerbate these effects, as EC can be deprotonated at high oxidative potentials to form H^+ , which could lead to further reaction of LiEDC and additional CO_2 evolution. [34,35]

Inner-SEI: Quantification of Hydrogen Evolution. As shown in Reaction R1, we propose that H_2 evolution coincides primarily with LiF deposition, with minor amounts of LiOH and Li_2O also being concomitantly deposited (see Reactions R2 and R3). These three components together make up the LiF-rich inner-SEI. We find in Figure 2a-d that LiPF_6 concentration has a significant impact on the amount of H_2 evolution. From 0.35 M to 1.2 M LiPF_6 , the H_2 evolution peak increases in height yet remains consistent in duration (~3.5 hrs). In contrast, the H_2 evolution signature for the 2.0 M LiPF_6 electrolyte is broader and persists for over five hours. The anomalous gassing behavior for the 2.0 M electrolyte is likely caused by the high viscosity of the 2.0 M electrolyte leading to slow wetting of the electrode pores or slow diffusion of H_2 through the electrolyte. Alternatively, the high concentration of Li^+ could alter the distribution of solvated species in solution (e.g., solvent separated ion pairs, contact ion pairs, aggregates, etc.), causing the reactive solvent (in this case, H_2O or HF) surrounding these different species to be reduced over a broad range of potentials.

The total H_2 evolved during cycling for each electrolyte is shown Figure 2e, revealing that the total H_2 evolved (and therefore the total thickness of the inner-SEI layer) increases with increasing LiPF_6 concentration. This trend can be rationalized by assuming the rate of HF formation in the electrolyte is first order with respect to LiPF_6 concentration, and we therefore observe a linear increase in H_2 evolution with increasing LiPF_6 concentration. This could occur if LiPF_6 reacts with either solvent species or residual H_2O over time to produce HF or other protic species. We also attempted to quantify LiF directly by extracting electrodes, rinsing them in D_2O , and performing ^{19}F nuclear magnetic resonance (NMR) on the rinsate with an external standard. While we observed a similar trend between the amount of LiF quantified using NMR and H_2 evolution, the NMR results were artificially high due to challenges with rinsing remnant LiPF_6 from the electrode prior to the D_2O rinse (PF_6^- would react with D_2O to form additional F^- in solution). The NMR results and method are described in Supporting Information Section S5, but not considered further here.

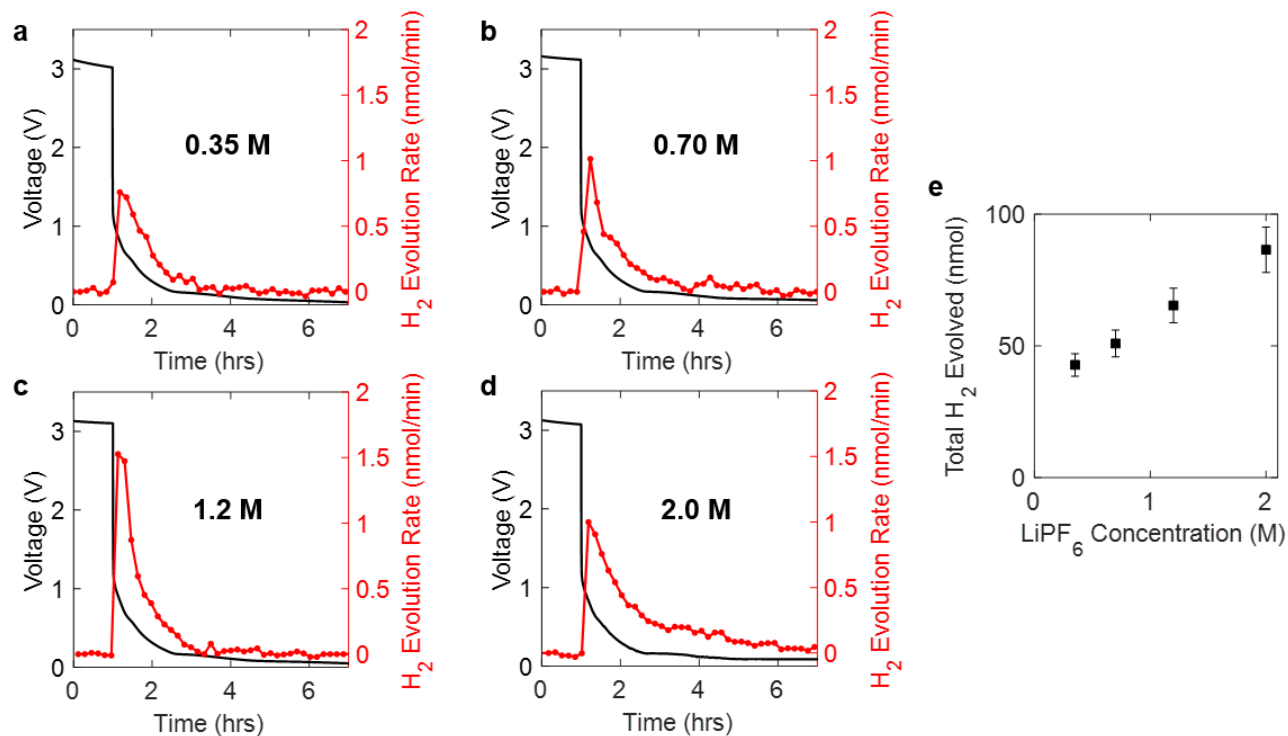


Figure 2: DEMS H₂ evolution in Li-graphite half cells cycled at C/10 with **a.** 0.35 M LiPF₆, **b.** 0.70 M LiPF₆, **c.** 1.2 M LiPF₆, and **d.** 2.0 M LiPF₆ electrolytes. **e.** Total H₂ evolved as a function of LiPF₆ concentration. Graphite electrodes were 12 mm in diameter with a graphite particle surface area of ~30 cm² (calculated based on 2.84 mAh/cm² lithiation capacity and an average graphite particle radius of 4 μm), and measurement error arising from integration of DEMS data is shown as ±10% in panel e.

DEMS was also performed on a cell using the same 1.2 M electrolyte in Figure 2c after it had been aged for about three months. As discussed previously, the extensive aging spurred additional HF formation in the electrolyte, which resulted in an almost fourfold increase in DEMS H₂ evolution over that observed in Figure 2c (see Supporting Information Section S2).

The implications of the inner-SEI thickness on battery operation are also important to consider. A thinner overall SEI may be advantageous for charge transfer, as Li⁺ must transport through the SEI layer to ultimately insert into graphite. The inner-SEI layer is generally thought to be compact, while the outer-SEI is thicker and more porous, [36] making the overall SEI thickness governed primarily by the outer-SEI. However, it is unclear exactly how Li⁺ transports through the SEI layer. It is likely that the Li⁺ remains at least partially solvated as it enters the outermost portion of the SEI, and it eventually strips the entirety of its solvation shell by the time it reaches the graphite surface. It is possible that the interface between the inner-SEI and outer-SEI is the point at which Li⁺ strips the last of its solvation shell, and Li⁺ migrates through the inner-SEI layer by hopping between F⁻, given that this inner-SEI is compact and likely would not accommodate a bulky solvated Li⁺. Depending on which mode of transport is slower (i.e., transport of partially solvated Li⁺ through the outer-SEI or Li⁺ hopping through the inner-SEI), SEI composition should be tailored accordingly.

Outer-SEI: Quantification of Solid Carbonates via DEMS and MST. The outer-SEI is comprised primarily of solid carbonates (such as LiEDC and LiEMC), and its initial formation coincides with C₂H₄ evolution from the reaction of EC to deposit LiEDC (see Reaction R6). As described previously, although LiEDC is thought to form initially, LiEDC can be further converted via an undetermined mechanism to LiEMC. [17] In light of this, the conversion of LiEDC to LiEMC and the outer-SEI composition generally warrant further investigation.

Our study reveals that LiPF₆ concentration plays a pivotal role in the formation of the outer-SEI layer, and we probe the formation of LiEDC via the evolution of C₂H₄ in DEMS. Figure 3a-d shows the C₂H₄ evolution signatures for all four tested electrolyte compositions. We find that the C₂H₄ evolution peak

height gradually decreases with increasing LiPF_6 concentration from 0.35 M to 1.2 M, but the peak duration remains similar. For the 2.0 M electrolyte, the peak is much broader and spans about six hours, which is similar to the H_2 evolution behavior for the 2.0 M electrolyte. We can thus apply similar reasoning to explain the broadness of both the H_2 and C_2H_4 evolution signatures for the 2.0 M electrolyte (i.e., electrolyte viscosity or Li^+ solvation effects).

Summing the total C_2H_4 evolved, we find in Figure 3e (blue squares) that C_2H_4 evolution monotonically decreases with increasing LiPF_6 concentration. This decrease in solid carbonate layer thickness may be attributed in part to the passivating effect of a thicker LiF-rich inner-SEI imparted by higher concentration electrolytes, which may inhibit some solid carbonate deposition. However, we find that after the 1.2 M electrolyte used in Figure 3c was aged three months, the H_2 evolution (and therefore the inner-SEI thickness) increased almost fourfold, yet the C_2H_4 evolution remained similar (within $\sim 2\%$, see Supporting Information Section S2), indicating the passivating effect of the inner-SEI is minor. Instead, the outer-SEI thickness appears to be related to an electrolyte property governed by the ratio of Li^+ to EC, presumably Li^+ solvation.

The ratios of EC to Li^+ in 0.35 M, 0.70 M, 1.2 M, and 2.0 M LiPF_6 in 3:7w EC:EMC electrolytes are 10.5, 5.3, 3.1, and 1.8, respectively. Since the inner solvation shell of Li^+ contains ~ 4 EC in solvent-separate ion pairs (SSIPs) when sufficient EC is present, [37] the 1.2 M and especially the 2.0 M electrolyte may contain a significant amount of contact ion pairs (CIPs) and aggregates (AGGs) with lower EC coordination numbers. It thus follows that, in both the 0.35 M and 0.70 M electrolytes, SSIPs with an inner solvation shell of ~ 4 EC reach the graphite surface. However, substantially more EC may be present in the outer solvation shell of the SSIPs in the 0.35 M electrolyte compared to the 0.70 M electrolyte, resulting in a larger amount of EC reduction and a thicker solid carbonate layer for the 0.35 M electrolyte. The difference between the 1.2 M and 2.0 M electrolytes is a bit more subtle, as in both cases there is not sufficient EC to fully coordinate each Li^+ in a ratio of 4 EC: Li^+ . We hypothesize that, in both the 1.2 M and 2.0 M cases, predominantly SSIPs with fourfold EC coordination migrate to the graphite surface, but slightly more AGGs (e.g., 2 Li^+ , 1 PF_6^- , and <4 EC) migrate to the graphite surface in the 2.0 M case compared to the 1.2 M case. This results in a modest decrease in the amount of EC reduction and solid carbonate layer thickness for the 2.0 M electrolyte compared to the 1.2 M electrolyte. CIPs (e.g., 1 Li^+ , 1 PF_6^- , and 3 EC) may also play a secondary role in SEI formation, but given that CIPs are overall charge neutral, these species are transported only via diffusion (rather than via diffusion and migration), and thus are not expected to be as prevalent as SSIPs and AGGs near the graphite surface. Similar logic about solvation and ion aggregation effects has been applied to explain the thin SEI layers formed on graphite with superconcentrated (greater than ~ 3 M) electrolytes. [38]

While C_2H_4 evolution provides a measure of the amount of LiEDC initially deposited, some LiEDC may be converted to other species. MST was therefore used to quantify the total amount of solid carbonate species that remained on each of the electrodes cycled in DEMS after the completion of a full formation cycle. As described in Supporting Information Section S1, under our definition of solid carbonates, LiEDC is counted as two solid carbonates, as there are two carbonate groups per LiEDC and two CO_2 are evolved from one LiEDC upon acid titration. LiEMC and Li_2CO_3 are likewise each counted as a single solid carbonate. The total amount of solid carbonates measured via CO_2 evolution during MST (green triangles) for each electrode cycled in DEMS is overlaid with the total C_2H_4 evolved during DEMS (blue circles) in Figure 3e. We find that the total amount of solid carbonates is greater than the amount of C_2H_4 evolved for each electrolyte composition, indicating that at least a portion of the SEI species remaining on the electrode after cycling are dicarbonates.

Further, we quantified the loss of initially deposited solid carbonates via the conversion of LiEDC to LiEMC by measuring the amount of CO_2 evolved in DEMS, as explained in Supporting Information Section S6. We plot the combined amount of CO_2 evolved in DEMS (which measures the extent of the LiEDC to LiEMC solid carbonate consumption mechanism) and the CO_2 evolved in MST (which measures the amount of solid carbonates remaining on the electrode after the formation cycle) for each electrolyte composition in Figure 3e (green circles). We find that the CO_2 evolved in DEMS is generally about one-tenth the amount of CO_2 evolved in MST, indicating the conversion of LiEDC to LiEMC represents a

small yet non-trivial contribution to the solid carbonate mass balance.

We now note that, if all initially deposited LiEDC remained intact on the electrode after the formation cycle, we would expect the ratio of CO₂ (MST) to C₂H₄ (DEMS) to be 2.0 (following the stoichiometry shown in Reactions R6 and S1.3 in Supporting Information Section S1). However, as shown in Figure 3f (black triangles), this ratio is ~1.5 for all electrolyte compositions tested, implying a ~25% reduction in the amount of solid carbonates after initial LiEDC deposition. If we assume LiEMC and Li₂CO₃ (both monocarbonates) are the sole products that LiEDC is converted to, this would imply monocarbonates comprise roughly 50% of the carbonates formed.

We know, however, that the conversion of LiEDC to LiEMC alone cannot fully explain the consumption of initially deposited LiEDC. We confirm this by combining the DEMS CO₂ evolution (which we propose coincides with conversion of LiEDC to LiEMC) with the CO₂ evolution during MST (which describes the solid carbonates remaining on the graphite surface after cycling) to arrive at a new ratio of CO₂ (MST+DEMS) to C₂H₄ (DEMS). This new ratio, which accounts for both solid carbonates remaining on the surface and LiEDC-to-LiEMC conversion, is ~1.65 for all electrolyte compositions. The fact that the ideal ratio of 2.0 CO₂ (MST+DEMS) to C₂H₄ (DEMS) is not reached implies that some amount of non-carbonate LiEDC reduction products (e.g., Li₂C₂ or lithium oxalate) are present, which is in agreement with previous studies. [8, 18] Comparing our measured CO₂ (MST+DEMS) to C₂H₄ (DEMS) ratio of ~1.65 to a theoretical ratio of 2.0 if all solid carbonates were accounted for, we calculate that ~18% of the initially deposited LiEDC is converted to non-carbonate species for all electrolyte compositions. The proposed Li₂C₂ and lithium oxalate non-carbonate species are highly reduced and therefore likely reside in close proximity to the reducing graphite surface, where they are interspersed with predominantly LiF in the inner-SEI layer.

Electrolyte aging was also found to significantly impact these results. The CO₂ (MST) to C₂H₄ (DEMS) ratio for the three-month aged 1.2 M electrolyte was ~0.94 (indicating the predominant presence of a monocarbonate — likely LiEMC — rather than a bicarbonate), and about four times more CO₂ was evolved during DEMS (indicating greater conversion of LiEDC to LiEMC) compared to the one-week aged electrolyte. The CO₂ (MST+DEMS) to C₂H₄ (DEMS) ratio for the three-month aged 1.2 M electrolyte was ~1.60, which in reasonable agreement with the one-week aged electrolytes (see Supporting Information Section S2). This implies that ~20% of the initially deposited LiEDC was converted to a non-carbonate species for the three-month aged electrolyte.

The insights gleaned from our measurements can help inform the next generation of the 'mosaic model' of the graphite SEI, [39] which originally posited that the SEI is composed of a LiF and Li₂O inner layer with a semicarbonate and Li₂CO₃ outer layer. Starting from the outermost layer and working inwards, our measurements indicate that LiEMC is likely the outermost constituent of the SEI, as the chemical reaction of LiEDC to LiEMC is expected to begin at the SEI-electrolyte interface and proceed inward (as shown in the inset to Figure 1d). Moving further inward, we then expect a layer predominantly comprised of LiEDC which has not been converted to other species, followed by LiEDC reduction products (such as Li₂C₂, oxalates, and alkoxides), which must be in contact with the reducing graphite surface and are therefore likely intertwined with the inner-SEI. The major constituent of the inner-SEI, whose deposition coincides with H₂ evolution, is LiF. Some LiOH and Li₂O may be interspersed in the inner-SEI as well, especially when using an electrolyte with high water content in the electrolyte. Although Li₂CO₃ was hypothesized to be abundant in the original mosaic SEI model, many studies since have found minimal [14, 33] or no Li₂CO₃. [22, 31, 32] Reactions R7 and R14 are potential pathways for Li₂CO₃ formation, but they are unlikely to occur to a great extent as discussed earlier. Possible origins of Li₂CO₃ are discussed in Supporting Information Section S7. Other previously reported SEI species, such as lithium alkoxides, could not be identified by our employed techniques but should be the subject of future work. [40]

SEI Evolution During a Single Fast Charge Cycle. With the SEI formed under each electrolyte composition characterized, we then explored how the initial SEI affects fast charge operation and how the SEI changes as a result of fast charge. Generally, a thinner initial SEI is preferred for fast charge applications, as overpotentials which arise from Li⁺ transport through the SEI layer can lead to Li plating and rapid capacity fade. We classify plated Li as yet another SEI component which is intertwined with the

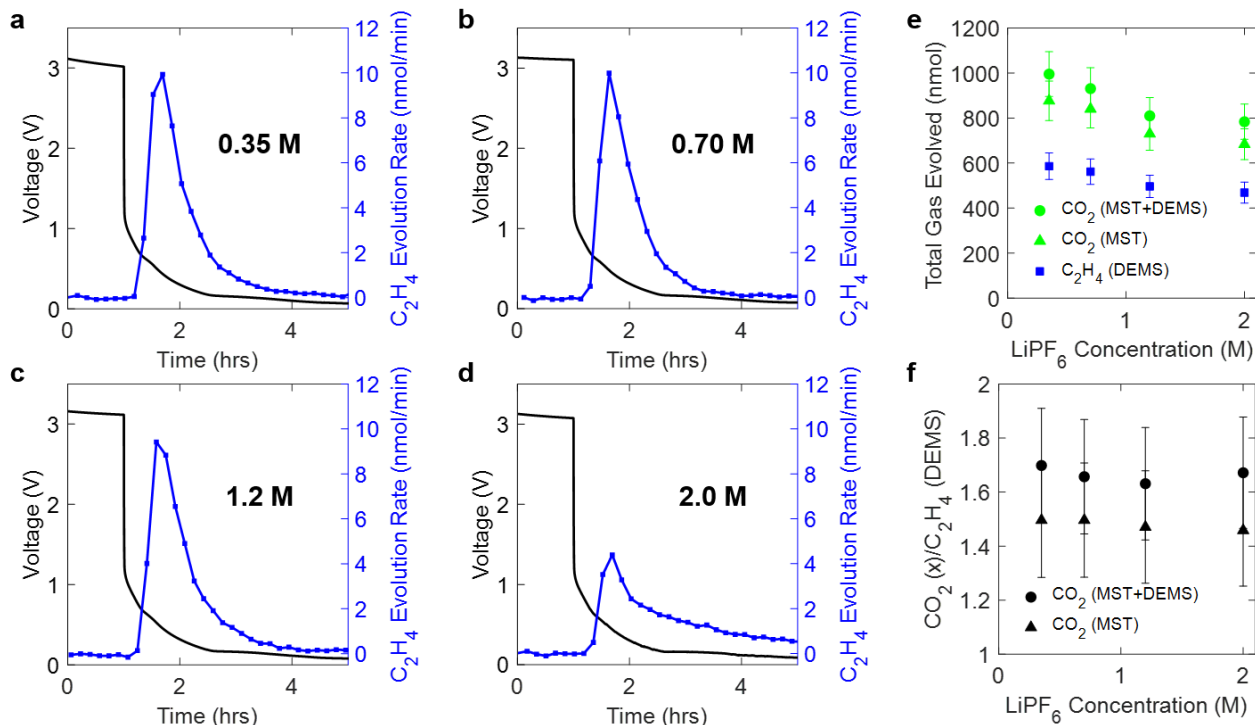


Figure 3: DEMS C_2H_4 evolution in Li-graphite half cells cycled at C/10 with **a.** 0.35 M $LiPF_6$, **b.** 0.70 M $LiPF_6$, **c.** 1.2 M $LiPF_6$, and **d.** 2.0 M $LiPF_6$ electrolytes. **e.** Total C_2H_4 evolved from DEMS (blue squares) overlaid with total CO_2 evolved from MST (green triangles) and combined CO_2 evolved from MST and DEMS (green circles) as a function of $LiPF_6$ concentration. Measurement error arising from integration of both DEMS and MST data is shown as $\pm 10\%$. **f.** Ratio of CO_2 evolved from MST to C_2H_4 evolved from DEMS (triangles) overlaid with ratio of combined CO_2 evolved from MST and DEMS to C_2H_4 evolved from DEMS (circles), with error propagated from panel e.

LiF, solid carbonates, and other species present in the initial SEI. Once plated, Li can undergo a number of processes:

1. It can be reversibly stripped from the graphite surface upon deintercalation.
2. It can chemically insert into graphite. [41,42]
3. It can become electronically isolated from the graphite, resulting in dead Li. [8]
4. It can react with other SEI components or with electrolyte to form additional SEI species. [8]

While processes 1 and 2 are reversible, processes 3 and 4 are irreversible and directly lead to capacity fade during fast charge cycling. Using MST, we quantify the amounts of dead Li and additional SEI formed after fast charge, and we compare the results against Li plating/stripping behavior predicted by an electrochemical model (see Supporting Information Section S1), [43,44] assuming a constant Li stripping efficiency of 70% as determined by previous work. [8] The cycling procedure outlined in Supporting Information Section S1, which allowed us to precisely identify the onset of Li plating, was used to collect the forthcoming electrochemical data.

The irreversible capacity of a single fast charge cycle to a given SOC (obtained from cycling data) is overlaid with the dead Li measured via MST and the model-predicted dead Li for the 0.35 M, 0.70 M, 1.2 M, and 2.0 M electrolytes in Figure 4a-d. It is clear from these data that the majority of capacity loss during a single fast charge cycle is due to dead Li formation, but some of the remaining capacity loss can be attributed to a slight increase in solid carbonates above the baseline amount observed after formation cycling, especially for the lower concentration electrolytes (see Supporting Information Section S8). As mentioned in Supporting Information Section S1, there is a baseline amount of ~ 300 nmol/cm² dead lithiated graphite present even after formation cycling due to the physical dislodgement of graphite

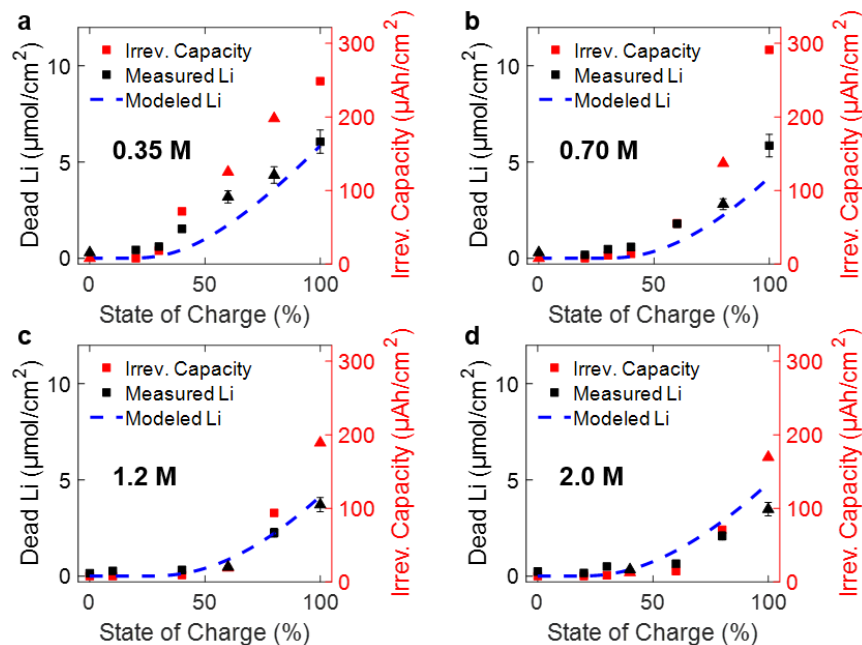


Figure 4: Experimental irreversible capacity (red markers, right y-axis) measured for a single fast charge cycle (4C rate) to a given SOC overlaid with dead Li measured via MST (black markers, left y-axis) and model predicted dead Li (blue dashed line) for **a.** 0.35 M LiPF₆, **b.** 0.70 M LiPF₆, **c.** 1.2 M LiPF₆, and **d.** 2.0 M LiPF₆ electrolytes. Measurement error arising from integration of MST data is shown as $\pm 10\%$, and irreversible capacity error bars are within the size of the data point ($\sim 1 \mu\text{Ah}/\text{cm}^2$). The left and right y-axes are scaled equivalently (i.e., $1 \mu\text{mol}/\text{cm}^2 \text{ Li} = 26.8 \mu\text{Ah}/\text{cm}^2$). Square markers denote data points collected with no replicates ($n=1$), and triangle markers denote the average of replicate data points ($n=2$).

particles from lithiation-induced volumetric changes of the particles during cycling. An increase in the amount of dead Li above this baseline amount is attributed to dead Li metal from fast charging.

The model fits the experimental dead Li data well for the 1.2 M electrolyte (as model parameters had been previously developed for this concentration), but generally underpredicts the amount of dead Li at a given SOC for the 0.35 M and 0.70 M electrolyte and overpredicts the amount of dead Li for the 2.0 M electrolyte. This discrepancy between model and experiment can be ascribed to changes in SEI impedance for cells formed with the electrolytes above and below 1.2 M, which the model as formulated does not capture. In Supporting Information Section S9, the SEI impedance is measured for each electrolyte composition using impedance spectroscopy in a three electrode configuration, [45] revealing that the SEI impedance generally decreases with increasing electrolyte salt content. Incorporating these SEI resistances into previously developed models which incorporate a graphite film resistance resulted in counterintuitive predicted Li plating behavior which did not match experimental results (as described in Supporting Information Section S1). This highlights the need for next generation models that more accurately and explicitly capture SEI effects as novel electrolyte formulations which impart beneficial SEI properties to enable fast charging are developed.

SEI Evolution During Multiple Fast Charge Cycles. We also measured the amount of dead Li, solid carbonates, and Li₂C₂ (see Supporting Information Section S3) on graphite electrodes that underwent multiple fast charge cycles. Following an analogous cycling procedure to that used in Figure 4, Li-graphite coin cells were cycled with three C/10 formation cycles followed by a 4C charge to 100% theoretical graphite SOC and a C/10 discharge to 1.5 V. This 4C fast charge cycle was then repeated up to a maximum of ten cycles. Representative voltage profiles during XFC are shown in Supporting Information Section S10, and plots of the Coulombic efficiencies (CEs) over the course of 10 cycles for each electrolyte composition are shown in Figure 5a. The amounts of dead Li and solid carbonates were quantified using MST for all tested electrolyte compositions and are shown in Figure 5b and 5c, respectively.

Figure Figure 5a shows that the CE is highest for the 1.2 M electrolyte over the course of 10 XFC cycles, and the the 0.70 M and 0.35 M electrolytes exhibit progressively lower CEs. The 2.0 M electrolyte begins with similar CE to the 1.2 M electrolyte, but the CE precipitously decreases after 5 XFC cycles,

such that the 2.0 M electrolyte exhibits the lowest CE on cycle 10 among all tested electrolytes.

Turning to titration results to explain the trends in CE, we find in Figure 5b that the dead Li remaining on the graphite electrode monotonically decreases with increasing electrolyte salt concentration. This trend is fairly well in line with that observed in Figure 4a-d for a single fast charge cycle, but the difference in dead Li amounts between electrolyte compositions is exacerbated after prolonged cycling. The reduced amount of dead Li is in part due to the lower SEI impedance for the higher concentration electrolytes as discussed previously, which leads to less Li plating for the higher concentration electrolytes. Additionally, the larger amount of LiF deposition when using the high concentration electrolytes likely improves the reversibility of Li plating/stripping, as numerous studies of Li plating/stripping on Cu indicate that LiF-depositing additives (such as fluoroethylene carbonate) impart a uniform columnar plated Li morphology and improve plating/stripping reversibility. [46,47] Interestingly, there is no obvious increase in the rate of dead Li accumulation for the 2.0 M electrolyte after 5 XFC cycles, indicating that dead Li is not the main cause of the precipitous CE decrease observed in Figure 5a.

We also probed the amount of additional solid carbonate deposition during fast charge, which occurs as a result of the reaction of plated Li metal with electrolyte solvent. [8] For small amounts of plated Li, the Li is well encapsulated by the existing SEI and has minimal contact with electrolyte, so minimal additional solid carbonate formation is observed (see Supporting Information Section S8). However, the accumulation of dead Li over the course of many cycles and the increased impedance of the SEI as dead Li accumulates may result in mossy Li which extends beyond the SEI and contacts the bulk electrolyte, resulting in additional solid carbonate deposition. We find in Figure 5c that the amount of solid carbonates deposited monotonically decreases with increasing electrolyte salt concentration. This is again consistent with the trend in solid carbonate amounts observed after a single fast charge cycle, indicating that Li⁺ solvation effects may limit the amount of EC reduction for the higher concentration electrolytes. Curiously, neither the dead Li nor the solid carbonate measurements explain the precipitous drop in CE observed for the 2.0 M electrolyte. We thus propose that this decrease in CE is due to LiF accumulation over XFC cycling, which we cannot directly measure with our titration technique. The increased amount of LiF in the SEI for high concentration electrolytes may also contribute to the lower amount of solid carbonate deposition. Since plated Li has been reported to have a more uniform, columnar morphology with a LiF-rich SEI, [46] higher concentration electrolytes (which impart LiF-rich SEIs) would reduce the plated Li surface area in contact with electrolyte and result in less solid carbonate formation.

Overall, the 1.2 M electrolyte exhibits the best capacity retention during XFC cycling among all tested electrolyte compositions and should be used for practical applications going forward. However, the 2.0 M electrolyte does provide insights which can be used to effectively tailor future electrolyte compositions for fast charge applications. Efforts should be focused on maintaining the beneficial properties of the 2.0 M electrolyte (less dead Li and solid carbonate deposition) while minimizing additional LiF deposition during XFC cycling. Utilizing electrolyte additives (e.g., fluoroethylene carbonate), which can impart beneficial SEI properties and are consumed during formation cycling, may provide an avenue to realize this goal.

Summary and Outlook. Using DEMS and MST, we completed a comprehensive, quantitative characterization of graphite SEI formation under electrolytes of varying LiPF₆ concentration. Our findings reveal that as LiPF₆ concentration increases, a thicker inner-SEI (rich in LiF) and a thinner outer-SEI (rich in alkyl carbonates) is formed, resulting in a thinner overall SEI. We also find that, although LiEDC is initially deposited, H₂O and HF convert LiEDC to LiEMC, and a host of other reactions convert LiEDC to non-carbonate species. The SEI resistance also plays a pivotal role in fast charge performance, as the thinnest, least resistive SEI formed under the 2.0 M electrolyte resulted in less dead Li than was predicted by an electrochemical model which did not incorporate explicit SEI effects. While some benefits of the 2.0 M electrolyte SEI were maintained over the course of multiple fast charge cycles (e.g., a decreased rate of dead Li formation and solid carbonate deposition), the 1.2 M electrolyte exhibited the best long-term capacity retention among all electrolyte compositions. Going forward, electrolyte engineering efforts should be focused on maintaining the benefits of highly concentrated electrolytes (e.g., by using electrolyte additives) while minimizing the capacity fade due to LiF deposition during prolonged XFC cycling. Finally, this work underscores the importance of appropriately incorporating SEI effects to accurately capture Li

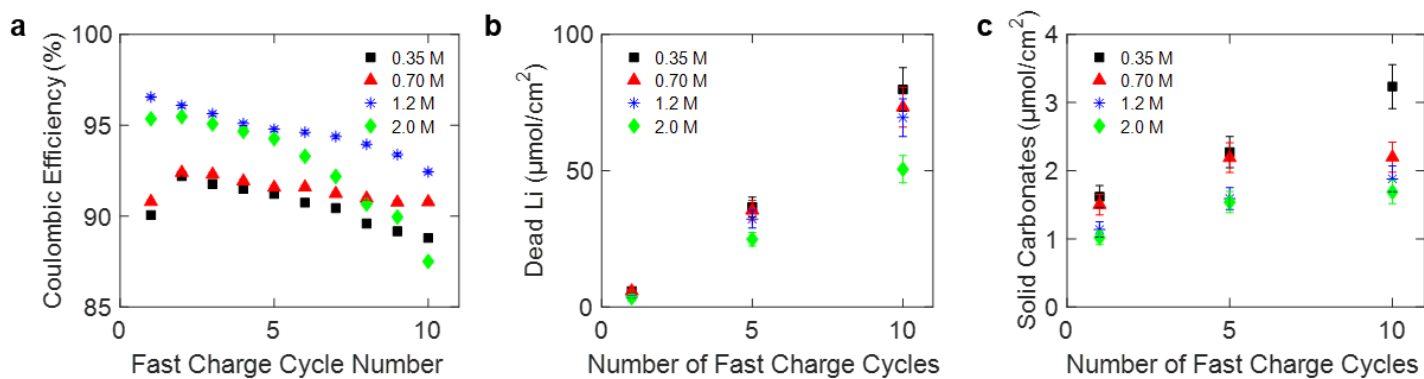


Figure 5: **a.** Coulombic efficiencies (CEs) over the course of ten 4C fast charge cycles for Li-graphite coin cells containing 0.35 M, 0.70 M, 1.2 M, and 2.0 M LiPF₆ in 3:7w EC:EMC electrolytes. Measurement error for the CE ($\sim 0.1\%$) is based on the time interval between data points during XFC. **b.** Quantification of dead Li via MST at varying stages of XFC cycling for each electrolyte composition. **c.** Quantification of solid carbonates via MST at varying stages of XFC cycling for each electrolyte composition. Measurement error arising from integration of MST data is shown as $\pm 10\%$. One measurement ($n=1$) was conducted for each data point shown in panels b and c.

plating behavior in next-generation electrochemical modeling frameworks.

Supporting Information

The following Supporting Information is available free of charge at the ACS website:

Complete complementary data sets for the experiments discussed in the main text along with detailed descriptions of the DEMS, MST, and modeling methods

Notes

The views expressed in this Letter do not necessarily represent the views of the DOE or the U.S. Government. The U.S. Government and the publisher, by accepting the article for publication, acknowledge that the U.S. Government retains a nonexclusive, paid-up, irrevocable, worldwide license to publish or reproduce the published form of this work, or allow others to do so, for U.S. Government purposes. The authors declare no competing financial interest.

Acknowledgements

This work was authored in part by the National Renewable Energy Laboratory, operated by Alliance for Sustainable Energy, LLC, for the U.S. Department of Energy (DOE) under Contract DE-AC36-08GO28308. Funding was provided by the U.S. DOE Office of Vehicle Technology Applied Battery Research and Extreme Fast Charge Program (XCEL). E.J.M. and D.E.B. acknowledge support from the National Science Foundation Graduate Research Fellowship Program (NSFGRFP) under Grant DGE 1106400 and H.K.B acknowledges support from the NSFGRFP under Grant DGE 1752814. We also acknowledge the CAMP facility at Argonne National Laboratory for providing the graphite electrodes used in this study. We thank Dr. Hasan Celik, Dr. Alicia Lund, and UC Berkeley's NMR facility in the College of Chemistry (CoC-NMR) for spectroscopic assistance. NMR instruments used in this work are supported in part by NIH S10OD024998.

References

- [1] Tongchao Liu, Lingpiao Lin, Xuanyuan Bi, Leilei Tian, Kai Yang, Jiajie Liu, Maofan Li, Zonghai Chen, Jun Lu, Khalil Amine, et al. In situ quantification of interphasial chemistry in Li-ion battery. *Nature nanotechnology*, 14(1):50–56, 2019.
- [2] Sara Renfrew. *Tracing Interfacial Reactivity of Lithium Transition Metal Oxides Through Outgassing*. PhD thesis, UC Berkeley, 2019.
- [3] Linxiao Geng, David L Wood III, Samuel A Lewis Sr, Raynella M Connatser, Mengya Li, Charl J Jafta, and Ilias Belharouak. High accuracy in-situ direct gas analysis of Li-ion batteries. *Journal of Power Sources*, 466:228211, 2020.
- [4] Paul G Kitz, Matthew J Lacey, Petr Novák, and Erik J Berg. Operando investigation of the solid electrolyte interphase mechanical and transport properties formed from vinylene carbonate and fluoroethylene carbonate. *Journal of Power Sources*, 477:228567, 2020.
- [5] Martin Lanz and Petr Novák. DEMS study of gas evolution at thick graphite electrodes for lithium-ion batteries: The effect of γ -butyrolactone. *Journal of power sources*, 102(1-2):277–282, 2001.
- [6] Martin Winter, R Imhof, F Joho, and Petr Novák. FTIR and DEMS investigations on the electroreduction of chloroethylene carbonate-based electrolyte solutions for lithium-ion cells. *Journal of power sources*, 81:818–823, 1999.
- [7] Hilmi Buqa, Andreas Würsig, Jens Vetter, ME Spahr, Frank Krumeich, and Petr Novák. SEI film formation on highly crystalline graphitic materials in lithium-ion batteries. *Journal of power sources*, 153(2):385–390, 2006.
- [8] Eric J McShane, Andrew M Colclasure, David E Brown, Zachary M Konz, Kandler Smith, and Bryan D McCloskey. Quantification of inactive lithium and solid–electrolyte interphase species on graphite electrodes after fast charging. *ACS Energy Letters*, 5(6):2045–2051, 2020.

- [9] Bryan D McCloskey, Donald S Bethune, Robert M Shelby, G Girishkumar, and Alan C Luntz. Solvents' critical role in nonaqueous lithium–oxygen battery electrochemistry. *The Journal of Physical Chemistry Letters*, 2(10):1161–1166, 2011.
- [10] Michael Stich, Mara Gottlinger, Mario Kurniawan, Udo Schmidt, and Andreas Bund. Hydrolysis of LiPF_6 in carbonate-based electrolytes for lithium-ion batteries and in aqueous media. *The Journal of Physical Chemistry C*, 122(16):8836–8842, 2018.
- [11] Michael Metzger, Benjamin Strehle, Sophie Solchenbach, and Hubert A Gasteiger. Hydrolysis of ethylene carbonate with water and hydroxide under battery operating conditions. *Journal of The Electrochemical Society*, 163(7):A1219, 2016.
- [12] Dusan Strmcnik, Ivano E Castelli, Justin G Connell, Dominik Haering, Milena Zorko, Pedro Martins, Pietro P Lopes, Bostjan Genorio, Thomas Østergaard, Hubert A Gasteiger, et al. Electrocatalytic transformation of HF impurity to H_2 and LiF in lithium-ion batteries. *Nature Catalysis*, 1(4):255–262, 2018.
- [13] Ken Tasaki, Katsuya Kanda, Shinichiro Nakamura, and Makoto Ue. Decomposition of LiPF_6 and stability of PF_5 in Li-ion battery electrolytes: Density functional theory and molecular dynamics studies. *Journal of the Electrochemical Society*, 150(12):A1628, 2003.
- [14] Philip Niehoff, Stefano Passerini, and Martin Winter. Interface investigations of a commercial lithium ion battery graphite anode material by sputter depth profile X-ray photoelectron spectroscopy. *Langmuir*, 29(19):5806–5816, 2013.
- [15] Vallabha Rao Rikka, Sumit Ranjan Sahu, Abhijit Chatterjee, PV Satyam, Raju Prakash, MS Ramachandra Rao, R Gopalan, and G Sundararajan. In situ/ex situ investigations on the formation of the mosaic solid electrolyte interface layer on graphite anode for lithium-ion batteries. *The Journal of Physical Chemistry C*, 122(50):28717–28726, 2018.
- [16] Chuntian Cao, Travis P Pollard, Oleg Borodin, Julian E Mars, Yuchi Tsao, Maria R Lukatskaya, Robert M Kasse, Marshall A Schroeder, Kang Xu, Michael F Toney, et al. Toward unraveling the origin of lithium fluoride in the solid electrolyte interphase. *Chemistry of Materials*, 33(18):7315–7336, 2021.
- [17] Luning Wang, Anjali Menakath, Fudong Han, Yi Wang, Peter Y Zavalij, Karen J Gaskell, Oleg Borodin, Dinu Iuga, Steven P Brown, Chunsheng Wang, et al. Identifying the components of the solid–electrolyte interphase in Li-ion batteries. *Nature chemistry*, 11(9):789–796, 2019.
- [18] Liwei Zhao, Izumi Watanabe, Takayuki Doi, Shigeto Okada, and Jun-ichi Yamaki. TG-MS analysis of solid electrolyte interphase (SEI) on graphite negative-electrode in lithium-ion batteries. *Journal of power sources*, 161(2):1275–1280, 2006.
- [19] Marco-Tulio Fonseca Rodrigues, Victor A Maroni, David J Gosztola, Koffi PC Yao, Kaushik Kalaga, Ilya A Shkrob, and Daniel P Abraham. Lithium acetylide: A spectroscopic marker for lithium deposition during fast charging of Li-ion cells. *ACS Applied Energy Materials*, 2(1):873–881, 2018.
- [20] Yixuan Wang, Shinichiro Nakamura, Makoto Ue, and Perla B Balbuena. Theoretical studies to understand surface chemistry on carbon anodes for lithium-ion batteries: Reduction mechanisms of ethylene carbonate. *Journal of the American Chemical Society*, 123(47):11708–11718, 2001.
- [21] Guorong V Zhuang, Kang Xu, Hui Yang, T Richard Jow, and Philip N Ross. Lithium ethylene dicarbonate identified as the primary product of chemical and electrochemical reduction of EC in 1.2 M $\text{LiPF}_6/\text{EC}:\text{EMC}$ electrolyte. *The Journal of Physical Chemistry B*, 109(37):17567–17573, 2005.
- [22] Guorong V Zhuang and Philip N Ross Jr. Analysis of the chemical composition of the passive film on Li-ion battery anodes using attenuated total reflection infrared spectroscopy. *Electrochemical and Solid State Letters*, 6(7):A136, 2003.

- [23] AM Andersson and Kristina Edström. Chemical composition and morphology of the elevated temperature SEI on graphite. *Journal of the Electrochemical Society*, 148(10):A1100, 2001.
- [24] Satu Kristiina Heiskanen, Jongjung Kim, and Brett L Lucht. Generation and evolution of the solid electrolyte interphase of lithium-ion batteries. *Joule*, 3(10):2322–2333, 2019.
- [25] Rebecca Bernhard, Michael Metzger, and Hubert A Gasteiger. Gas evolution at graphite anodes depending on electrolyte water content and SEI quality studied by on-line electrochemical mass spectrometry. *Journal of The Electrochemical Society*, 162(10):A1984, 2015.
- [26] Paul G Kitz, Petr Novák, and Erik J Berg. Influence of water contamination on the SEI Formation in Li-ion cells: An operando EQCM-D study. *ACS applied materials & interfaces*, 12(13):15934–15942, 2020.
- [27] Doron Aurbach, Yosef Gofer, Moshe Ben-Zion, and Pinchas Aped. The behaviour of lithium electrodes in propylene and ethylene carbonate: The major factors that influence Li cycling efficiency. *Journal of Electroanalytical Chemistry*, 339(1-2):451–471, 1992.
- [28] L Gireaud, S Grugeon, S Laruelle, S Pilard, and J-M Tarascon. Identification of Li battery electrolyte degradation products through direct synthesis and characterization of alkyl carbonate salts. *Journal of the Electrochemical Society*, 152(5):A850, 2005.
- [29] Kang Xu, Guorong V Zhuang, Jan L Allen, Unchul Lee, Sheng S Zhang, Philip N Ross Jr, and T Richard Jow. Syntheses and characterization of lithium alkyl mono- and dicarbonates as components of surface films in Li-ion batteries. *The Journal of Physical Chemistry B*, 110(15):7708–7719, 2006.
- [30] Daniel M Seo, Dinesh Chalasani, Bharathy S Parimalam, Rahul Kadam, Mengyun Nie, and Brett L Lucht. Reduction reactions of carbonate solvents for lithium ion batteries. *ECS Electrochemistry Letters*, 3(9):A91, 2014.
- [31] Doron Aurbach, Boris Markovsky, Alexander Rodkin, Miriam Cojocaru, Elena Levi, and Hyeong-Jin Kim. An analysis of rechargeable lithium-ion batteries after prolonged cycling. *Electrochimica Acta*, 47(12):1899–1911, 2002.
- [32] Mengyun Nie, Dinesh Chalasani, Daniel P Abraham, Yanjing Chen, Arijit Bose, and Brett L Lucht. Lithium ion battery graphite solid electrolyte interphase revealed by microscopy and spectroscopy. *The Journal of Physical Chemistry C*, 117(3):1257–1267, 2013.
- [33] Anna M Andersson, A Henningson, Hans Siegbahn, Ulf Jansson, and Kristina Edström. Electrochemically lithiated graphite characterised by photoelectron spectroscopy. *Journal of Power Sources*, 119:522–527, 2003.
- [34] Yang Yu, Pinar Karayaylali, Yu Katayama, Livia Giordano, Magali Gauthier, Filippo Maglia, Roland Jung, Isaac Lund, and Yang Shao-Horn. Coupled LiPF₆ decomposition and carbonate dehydrogenation enhanced by highly covalent metal oxides in high-energy Li-ion batteries. *The Journal of Physical Chemistry C*, 122(48):27368–27382, 2018.
- [35] Thomas M Østergaard, Livia Giordano, Ivano E Castelli, Filippo Maglia, Byron K Antonopoulos, Yang Shao-Horn, and Jan Rossmeisl. Oxidation of ethylene carbonate on Li metal oxide surfaces. *The Journal of Physical Chemistry C*, 122(19):10442–10449, 2018.
- [36] William Huang, Peter M Attia, Hansen Wang, Sara E Renfrew, Norman Jin, Supratim Das, Zewen Zhang, David T Boyle, Yuzhang Li, Martin Z Bazant, et al. Evolution of the solid–electrolyte interphase on carbonaceous anodes visualized by atomic-resolution cryogenic electron microscopy. *Nano letters*, 19(8):5140–5148, 2019.
- [37] Narendra Kumar and Jorge M Seminario. Lithium-ion model behavior in an ethylene carbonate electrolyte using molecular dynamics. *The Journal of Physical Chemistry C*, 120(30):16322–16332, 2016.

- [38] Jianming Zheng, Joshua A Lochala, Alexander Kwok, Zhiqun Daniel Deng, and Jie Xiao. Research progress towards understanding the unique interfaces between concentrated electrolytes and electrodes for energy storage applications. *Advanced Science*, 4(8):1700032, 2017.
- [39] E Peled, D Golodnitsky, and G Ardel. Advanced model for solid electrolyte interphase electrodes in liquid and polymer electrolytes. *Journal of the Electrochemical Society*, 144(8):L208, 1997.
- [40] Pallavi Verma, Pascal Maire, and Petr Novák. A review of the features and analyses of the solid electrolyte interphase in Li-ion batteries. *Electrochimica Acta*, 55(22):6332–6341, 2010.
- [41] C Uhlmann, J Illig, M Ender, R Schuster, and E Ivers-Tiffée. In situ detection of lithium metal plating on graphite in experimental cells. *Journal of Power Sources*, 279:428–438, 2015.
- [42] Zachary M Konz, Eric J McShane, and Bryan D McCloskey. Detecting the onset of lithium plating and monitoring fast charging performance with voltage relaxation. *ACS Energy Letters*, 5(6):1750–1757, 2020.
- [43] Andrew M Colclasure, Tanvir R Tanim, Andrew N Jansen, Stephen E Trask, Alison R Dunlop, Bryant J Polzin, Ira Bloom, Dave Robertson, LeRoy Flores, Michael Evans, et al. Electrode scale and electrolyte transport effects on extreme fast charging of lithium-ion cells. *Electrochimica Acta*, 337:135854, 2020.
- [44] Andrew M Colclasure, Alison R Dunlop, Stephen E Trask, Bryant J Polzin, Andrew N Jansen, and Kandler Smith. Requirements for enabling extreme fast charging of high energy density Li-ion cells while avoiding lithium plating. *Journal of the Electrochemical Society*, 166(8):A1412, 2019.
- [45] D. E. Brown, E. J. McShane, Z. M. Konz, K. B. Knudsen, and B. M. McCloskey. Detecting onset of lithium plating during fast charging of Li-ion batteries using operando electrochemical impedance spectroscopy. *Cell Reports Physical Science*, 36(2):100589, 2021.
- [46] Chengcheng Fang, Jinxing Li, Minghao Zhang, Yihui Zhang, Fan Yang, Jungwoo Z Lee, Min-Han Lee, Judith Alvarado, Marshall A Schroeder, Yangyuchen Yang, et al. Quantifying inactive lithium in lithium metal batteries. *Nature*, 572(7770):511–515, 2019.
- [47] Xue-Qiang Zhang, Xin-Bing Cheng, Xiang Chen, Chong Yan, and Qiang Zhang. Fluoroethylene carbonate additives to render uniform Li deposits in lithium metal batteries. *Advanced Functional Materials*, 27(10):1605989, 2017.